The molecular picture for Amplified Spontaneous Emission of star-shaped functionalized-truxene derivates

Lin Ma [#a], Zhaoxin Wu [#*a], Guijiang Zhou [*b], Fang Yuan [a], Yue Yu [a], Chunliang Yao [b], Shuya Ning [a],

Xun Hou [a], Yu Li [c], Shufeng Wang [c] and Qihuang Gong [c]

[a] Key Laboratory of Photonics Technology for Information, School of Electronic and Information

Engineering, Xi'an Jiaotong University, Xi'an 710049, PR China

[b] Department of Chemistry, School of Science, Xi'an Jiaotong University, Xi'an 710049, PR China

[c] State Key Laboratory for Mesoscopic Physics and Department of Physics, Peking University,

Beijing 100871, PR China

[*] Corresponding author. zhaoxinwu@mail.xjtu.edu.cn, Tel: +86-29-82664867; Fax: +86-29-82664867

[*] Corresponding author. zhougj@mail.xjtu.edu.cn, Tel: +86-29-82663914; Fax: +86-29-82663914

[#] These authors contributed equally to this work.

Abstract

Organic optical gain materials are the basis for the organic solid-state lasers. However, the fundamental mechanism for Amplified Spontaneous Emission (ASE) is absent. Herein, three star-shaped molecules based on a truxene core with π-conjugated arms are studied to illuminate the influence of the molecular structure on ASE performance. We found that the three compounds demonstrated different ASE characteristics. The strong conjugated linkage in the molecular arms enhanced ASE, while the attenuated conjugated linkage deteriorates ASE for the given molecular structures. Based on the theoretical analysis, the conjugative coupling suppresses the low-frequency vibration, which is beneficial to the formation of effective "four-level" energy system for ASE. On the contrary, the poor conjugative coupling brings out a mass of low-frequency modes, hence, continuous vibronic energy sublevels will ruin the molecular "four-level" energy system. Our study presented a clear picture to clarify the ASE mechanism and offer valuable guidance for the design of new organic optical gain materials.

1. Introduction

Organic semiconductor materials for lasing have attracted considerable attention recently because of their outstanding optoelectronic properties and solution processability. [1-8] Besides, organic semiconductor materials, expected to be the promising candidates for solid state laser, possess broad emission spectra and can be tuned over a wide wavelength range. [9-13] In order to achieve the lasing with the broad tunable wavelength and lower optically pump threshold, a mass of organic molecules have been found or synthesized to be used as the gain medium in laser and optical amplifier applications, such as nitrogen-containing heterocyclic emitters (4,4'-bis(9-carbazolyl)-2,2'-biphenyl (CBP) and the derivatives), ladder polymers (poly(2-methoxy-5-(2'-ethylhexyloxy)-1,4-phenylene vinylene) (MEH-PPV), poly(2-butyl-5-(2'-ethylhexyl)-1,4-phenylene vinylene) (BuEH-PPV) etc.), perpendicular spirobifluorene derivates, pyrene-cored dendrimers, truxene-cored star-shaped macromolecules, perilenediimide derivatives (PDIs), and spiropyran biopolymer system deoxyribonucleic acid (DNA) with high thermal stability and good solubility. [9, 14-20] Although these organic molecules show significant lasing performances, from the molecular structure point of view, the fundamental mechanism for ASE is absent, making their elucidation a major issue. In theory, previous works only focused on electronic structures in electronic states, photophysics properties, optical spectra and Raman spectroscopy. [21-24] These theoretical works fail to provide a reasonable explanation for ASE characteristics. For the improved understanding of ASE characteristics, Adachi and co-authors reported a great deal of extremely low ASE

threshold (as low as (0.11 ± 0.05) $\mu J/cm^2$) materials, [25-30] and their works pointed out that the ASE threshold is closely correlated with the radiative decay rate k_f and signified a larger k_f results in a larger ASE gain. However, these works seemingly were confined to experimental discussion for ASE and did not provide the fingerprint of intrinsic ASE mechanism for organic semiconductor molecules. Up to now, limited theoretical explanations were proposed from the molecular structure and energy level point of view to better understand the ASE properties.

In this paper, three star-shaped molecules based on a truxene core with π-conjugated arms [31] (see Figure 1) are studied to illuminate the influence of the molecular structure on ASE performance. Truxene-cored with spirobifluorene arms (Tr1) showed optical gain with ASE threshold of 156 $\mu J/cm^{-1}$. Introducing the thiophene (Tr2) between truxene core and spirobifluorene arms, the ASE threshold down to 83 $\mu J/cm^{-1}$. However, the ASE disappeared when thiophene was replaced by N-ethylcarbazole (Tr3). Base on DFT/TDDFT calculations, we found that the introduced thiophene improves conjugative coupling and suppresses low-frequency vibrational modes, just like "locks" trxuene core and spirobifluorene arms together. Meanwhile, high-frequency CC stretching modes were enhanced, shown in Raman spectra. The decreased low-frequency modes and enhanced high-frequency modes are beneficial to form effective "four-level" energy system for ASE. On the contrary, the embedded N-ethylcarbazole moieties fail to modify conjugative coupling and bring out a mass of strongly elongated low-frequency modes, hence, continuous vibronic energy sublevels would ruin the molecular "four-level" energy system.

2. Results and Discussion
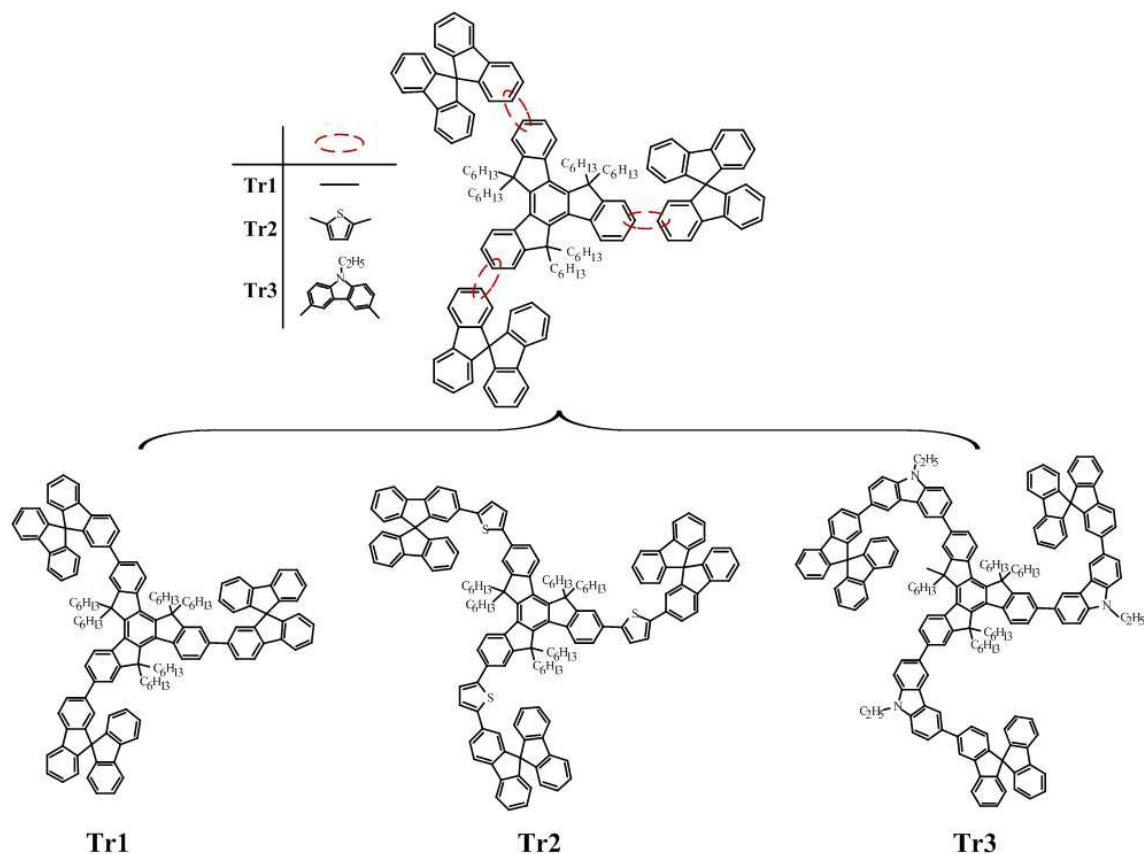
Figure 1 Chemical structures of truxene-cored star-shaped compounds Tr1, Tr2 and Tr3.

Figure 1 shows the chemical structures of the three star-shaped compounds, comprising a truxene core and different arms: directly linked through single bond (Tr1), linked via thiophene unit (Tr2) and N-ethylcarbazole unit is embedded at the same position instead (Tr3).

2.1. Photoluminescence and Absorption Spectra
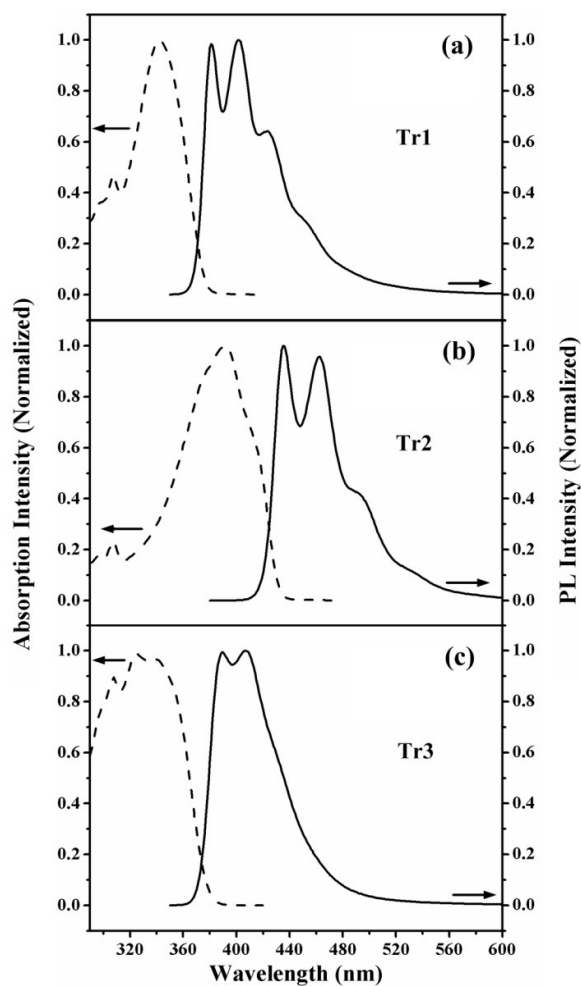
Figure 2 Normalized absorption spectra (dashed lines, left ordinate) and normalized photoluminescence emission (solid lines, right ordinate) spectra for doped thin film samples of (a) Tr1, (b) Tr2, (c) Tr3.

Figure 2 shows the normalized absorption and photoluminescence (PL) spectra for thin films of three compounds. The spectra for Tr2 are red-shifted with respect to those of Tr1 and Tr3, which is an indication of extended conjugation for Tr2. Interestingly, introduced N-ethylcarbazole (Tr3) does not cause apparent movement of spectra. Moreover, the PL spectra of Tr1 and Tr2 possess resolved vibrational progression,

which corresponds to a four-level energy system, but that of Tr3 only has an unresolved

longer-wavelength shoulder. The specific parameters were shown in Table 1. In

addition, the observed large Stokes shift (0.64 eV) between absorption and PL emission

peaks for Tr3 suggests that there may be a significant geometric relaxation following

excitation of this compound, this is discussed in more detail below.

2.2. Amplified Spontaneous Emission Properties
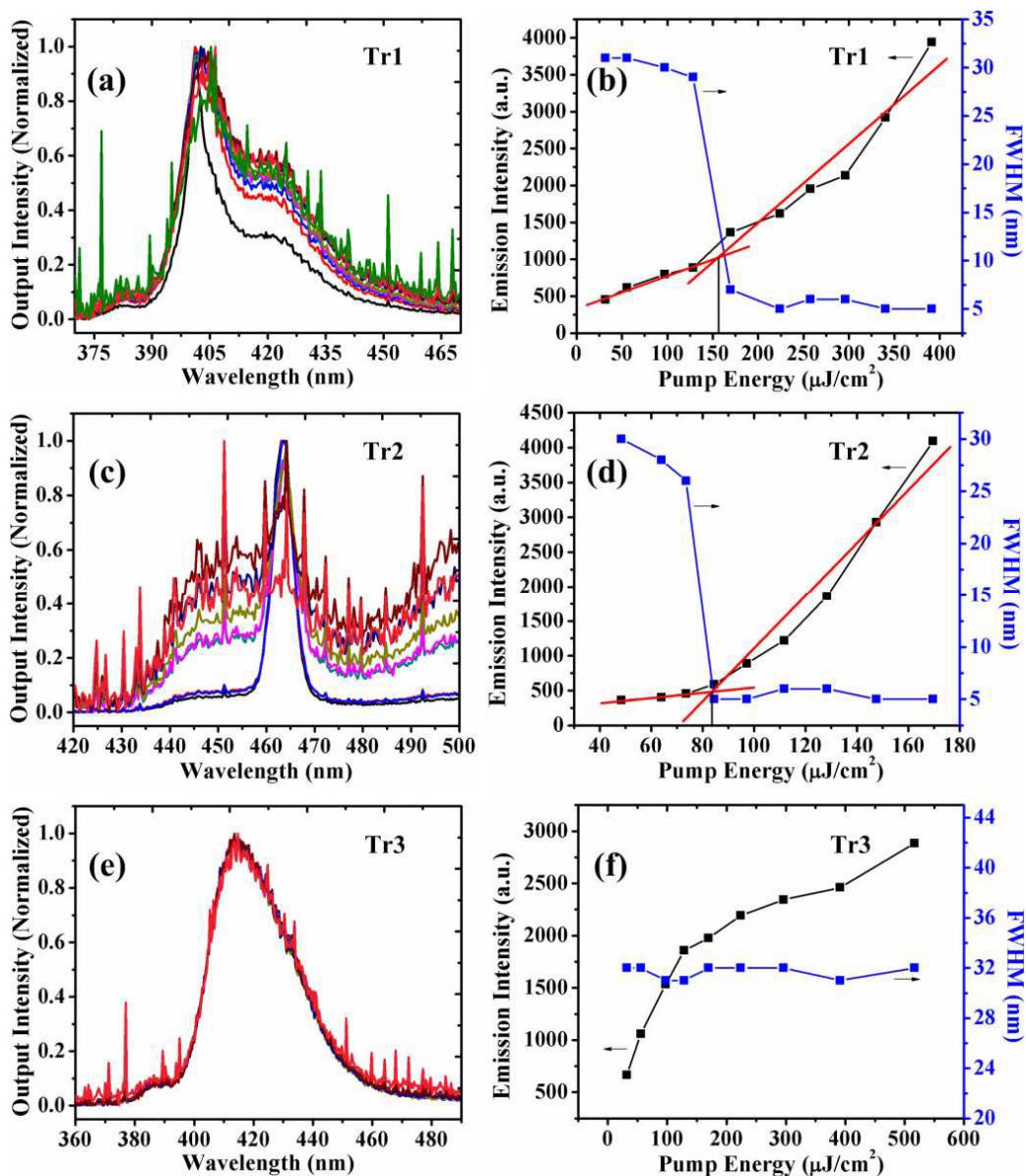
Figure 3 The edge-emission spectra of doped thin films for Tr1 (a), Tr2 (c) and Tr3 (e) excited by different energy. Output intensity at λ_{ASE} and Full Widths at Half-maximum (FWHM) as a function of pump energy for Tr1 (b), Tr2 (d) and Tr3 (f).

Above certain excitation densities, we observed ASE for Tr1 and Tr2, with line-narrowed spectra (see Figure 3(a) and Figure 3(c)) peaked at 401.2 nm and 463.4 nm separately, close to the 0-1 vibronic peak of the PL emission. This corresponds to a

four-level vibronic system allowing population inversion operation. [32] Figure 3(b) and 3(d) shows the full-width at half-maximum (FWHM) linewidth of the emission spectrum, and relative output power, as a function of the pump intensity. The ASE threshold of Tr2 (83 $\mu J/cm^2$) was reduced by one time versus that of Tr1 (156 $\mu J/cm^2$).We found that the FWHM dropped dramatically to 5 nm when pumping above ASE thresholds. The reduction in linewidth occurs because the net gain is maximal near the 0-1 vibronic peak of the PL emission spectrum and thus the spectrum exhibits gain narrowing as the pump intensity increases. In contrast, the FWHM of Tr3 was around 33 nm, and there was no significant gain-narrowing even under typical pumping conditions (see Figure 3(e) and 3(f)). ASE is also very useful as the means to determine the available optical gain and waveguide losses using the variable stripe technique. [33] The details were shown in Figure S1 in Supporting Information. In the ASE measurements, the spontaneous emission from unrelated single molecules is amplified as it travelling in slab waveguide (organic thin film) and the output beam is incoherent light, which is differ from superfluorescence properties (cooperative spontaneous emission). [3]

Table 1 Numerical values for physical properties and ASE characteristics of three compounds.

Compound	$\lambda_{PL(0-0)}$ [a] (nm)	$\lambda_{PL(0-1)}$ [b] (nm)	$\lambda_{PL(0-2)}$ [c] (nm)	λ_{ASE} [d] (nm)	E_{th} [e] ($\mu J/cm^2$)	FWHM [f] (nm)	ΔG_{ASE} [g] (cm^{-1})	α [h] (cm^{-1})	Φ_{PL} [i] (%)	τ_f [j] (ns)	k_f [k] ($10^8 \ s^{-1}$)
Tr1	381	401	423	401.2	156	5	19	3.2	66	1.48	4.5
Tr2	435	463	490	463.4	83	5	32	3.4	52	0.43	12.1
Tr3	389	407	–	–	–	–	–	–	35	2.19	1.5

[a] Fluorescence 0-0 vibronic transition peak wavelength. [b] Fluorescence 0-1 vibronic transition peak wavelength. [c] Fluorescence 0-2 vibronic transition peak wavelength. [d] ASE peak wavelength. [e] Excitation power threshold for ASE. [f] Full width at half maximum (FWHM) of ASE spectrum. [g] ASE gain. [h] ASE loss coefficient. [i] Determined in CH_2Cl_2 using quinine sulfate (Φ_{PL} = 56% in 1.0 M H_2SO_4 solution) as standard. [j] Transient PL lifetime. [k] Radiative decay rate k_f was calculated by Φ_{PL}/τ_f.

2.3. Photoluminescence Quantum Yield and Lifetime

The PLQY measurements gave Φ_{PL}=66% for Tr1 and Φ_{PL}=52% for Tr2, signify the radiative decay process is dominant. However, the significantly reduced PLQY for Tr3 (Φ_{PL}=35%) may arise from a geometric relaxation following excitation, which then directly competes with the emission, namely non-radiative decay processes following absorption transition.
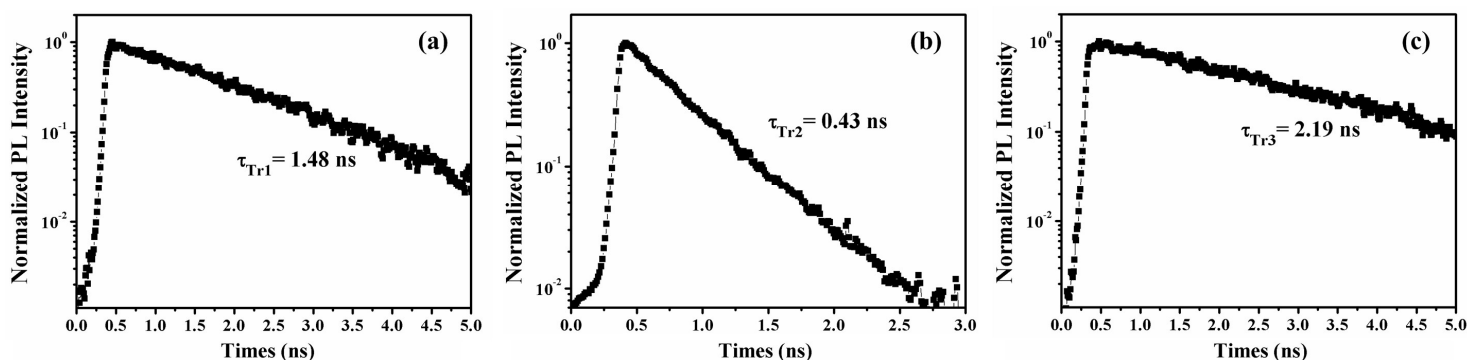

Figure 4 Normalized PL decay transients for (a) Tr1, (b) Tr2 and (c) Tr3 under 360 nm pulsed excitation.

PL transient decays measured results for doped films of three compounds are presented in Figure 4. The results for these compounds allow us to adopt a numerical convolution approach to extract the excited state lifetime. The close to single

exponential decays are evident for three compounds with excited state lifetimes τ_f =1.48

for Tr1, τ_f =0.43 for Tr2 and τ_f =2.19 for Tr3 respectively, listed in Table 1. The

lifetimes for Tr2 can compared to the parent truxene core T3 ($\tau_f \approx$ 0.33 ns) and T4 ($\tau_f \approx$

0.6 ns). [25, 34]

The radiative decay rate k_f is calculated by Φ_{PL}/τ_f. Table 1 demonstrate that Tr2 with

the lowest ASE threshold owns the highest radiative decay rate k_f =12.1×10^8 s^{-1}, which

arising from a high PLQY (Φ_{PL}) and a short transient lifetime (τ_f). For Tr1, a rather high

ASE threshold corresponds to an intermediate value of k_f (4.5×10^8 s^{-1}), while, Tr3 with

no ASE performance shows the lowest value (k_f =1.5×10^8 s^{-1}). The results give

indicative of the fact that low ASE thresholds originate from the large radiative decay

rate. The absence of ASE in the Tr3 compound is intriguing and has to be fully

understood.

2.4. Theoretical Molecular Geometries and Electronic Transitions

(a)

(b)
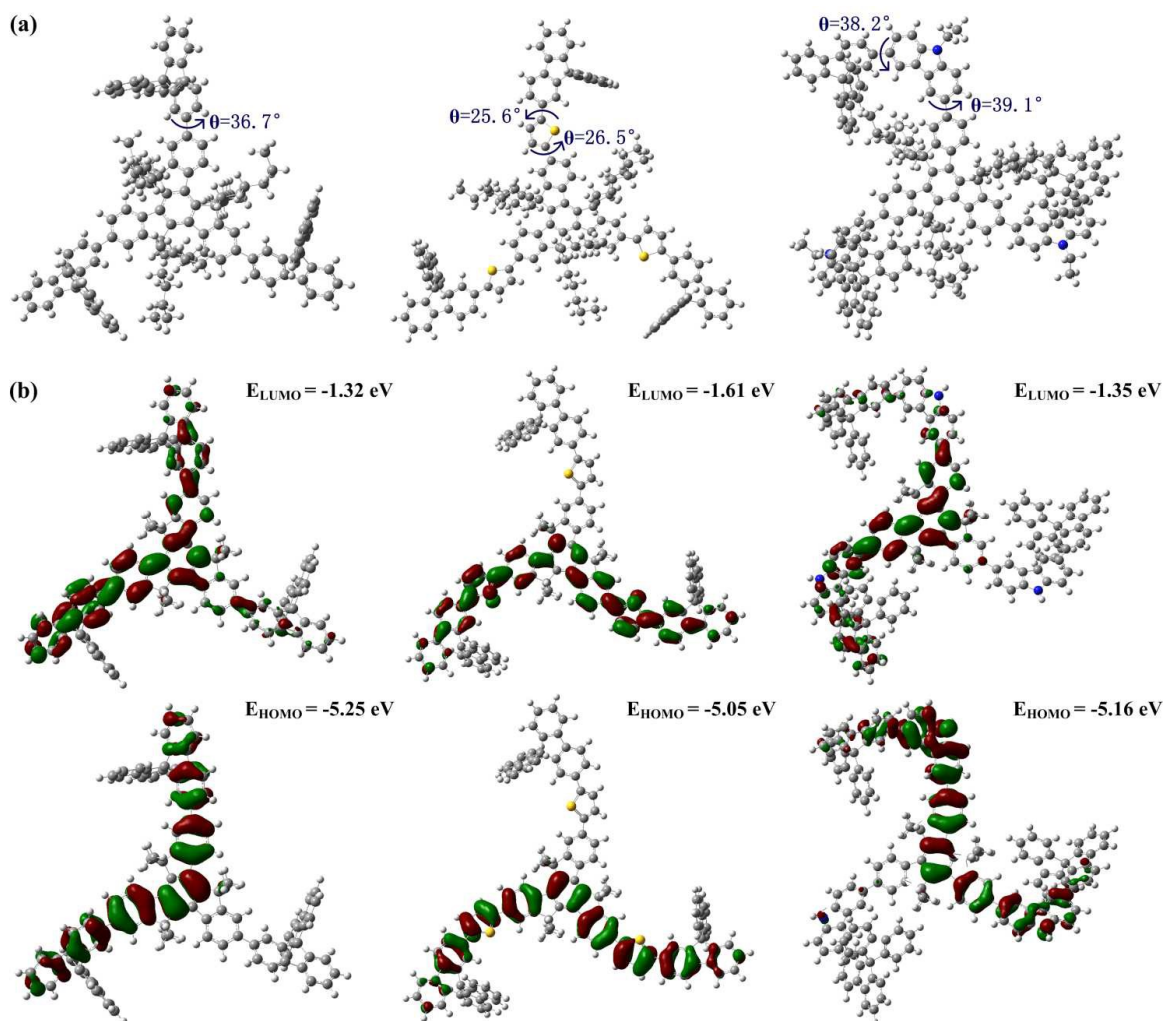
Figure 5 Optimized geometries (a) and Frontier Molecular Orbital (b) for three compounds.

To provide insight into the influence of the molecular structures on the ASE characteristics, we performed geometry optimizations within the framework of the DFT/TDDFT, using B3LYP/6-31G(d, p) level.

DFT/TDDFT calculations were performed on all compounds to gain insight into the optical features. Figure 5 demonstrates the optimized geometries for three compounds. In the calculations, the dihedral angle θ exists between truxene core and arms, as well

as the conjugated units in arms. For Tr1, the θ between truxene core and spirobifluorene

is optimized to be 36.7°. Introduced π-conjugated thiophene for Tr2 extends molecular

sterical dimension but weakens the steric hindrance, [35] hence, reduced θ (26.5° and

25.6°) enhances the conjugation coupling. Inversely, the N-ethylcarbazole (Tr3) fails to

decrease θ (38.2° and 39.1°) because the prominent steric interactions between

N-ethylcarbazole and other moieties. The conjugative coupling has not been improved

and the torsion of molecular skeleton would hamper electronic couplings.

The molecular geometry validly effects the electronic density distribution, which was

calculated eliminated the C_6H_{13} side chains, [36] presented in Figure 5(b). For all

compounds, HOMOs are localized on two of molecule arms and truxene core partially.

The large overlap for Tr2 mainly derives from two thiophene/spirobifluorene arms and

adjacent fluorene in truxene core due to enhanced conjugation, making for high k_f, and

it is similar for Tr1. However, LUMO of Tr3 is localized on two fluorene units in

truxene core chiefly, while HOMO is localized on the N-ethylcarbazole and adjacent

fluorene in truxene core. The overlap deriving from the partial truxene core is evident as

are low k_f for Tr3 compared to Tr1 and Tr2, shown in Table 1.

2.5. Transition Energies and Oscillator Strength

In order to further understand the optical properties for the three compounds. Base on

the optimized geometries, we have undertaken TDDFT calculations to further research

into the specific electronic transition of Tr1, Tr2 and Tr3 to deeply understand the

optical properties, shown in Table 2. The oscillator strength indicates the strength of

electronic transition. Tr2 presents a strong electronic transition compared to Tr1 and Tr3,

which benefits the ASE performance. As discussed above, the weak transition strength

for Tr3 dues to the small overlap integral between HOMO and LUMO compared to that

of the other two compounds (see Figure 5(b)). In addition, the weaker oscillator strength

would be expected to bring out a smaller radiative decay rate, shown in Table 1. More

detailed examinations are required to reveal the factors, which influences the ASE

properties based on the analysis of vibronic transitions and energy level system.

Table 2 Photophysics parameters obtained by TD-DFT method for Tr1, Tr2 and Tr3 at the B3LYP/6-31G(d, p) based on optimized geometries.

Compound	E^a (eV)				f^b
	absorption		emission		
	experiment	theory	experiment	theory	
Tr1	3.63	3.57	3.26	3.29	1.6782
Tr2	3.17	3.13	2.86	2.85	2.6574
Tr3	3.83	3.76	3.19	3.13	1.0115

[a] Vertical excitation energies. [b] Oscillator strength for emission.

2.6. Raman Spectra and Vibrational Modes
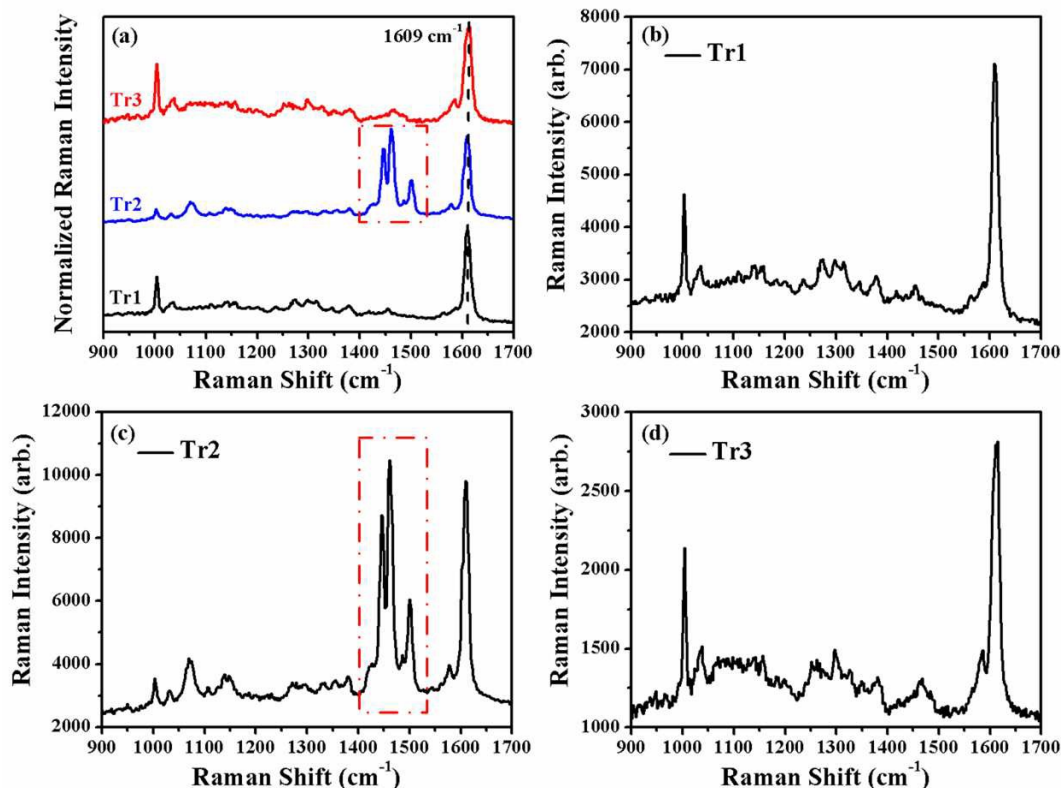
Figure 6 Normalized Raman spectra (a) and Raman spectra for Tr1 (b), Tr2 (c) and Tr3 (d).

The Raman spectra (see Figure 6) for three compounds share a common high-frequency mode on ≈1609 cm^{-1} (highlighted by vertical dashed line in Figure 6(a)), carbon-carbon ring stretching modes in typical conjugated structures. For Tr2, distinct

three high-frequency Raman peaks come out on ≈1446 cm^{-1}, 1462 cm^{-1} and 1501 cm^{-1} (see red dashed rectangle in Figure 6(a) and (c)), corresponding to in-plane ring skeleton stretching in π-conjugated units (truxene core, thiophene and spirobifluorene), which can be rationalized on the basis that the introduction of plane thiophene units generate some strong vibration high-frequency modes. In addition, we observe that as the thiophene was embedded, the Raman intensity increases by an order of magnitude, while, the N-ethylcarbazole weaken the Raman intensity instead. For Tr3, the twist molecular skeletons reduce conjugation, removing a substantial restoring force and resulting in the softening of high-frequency modes. [37, 38]
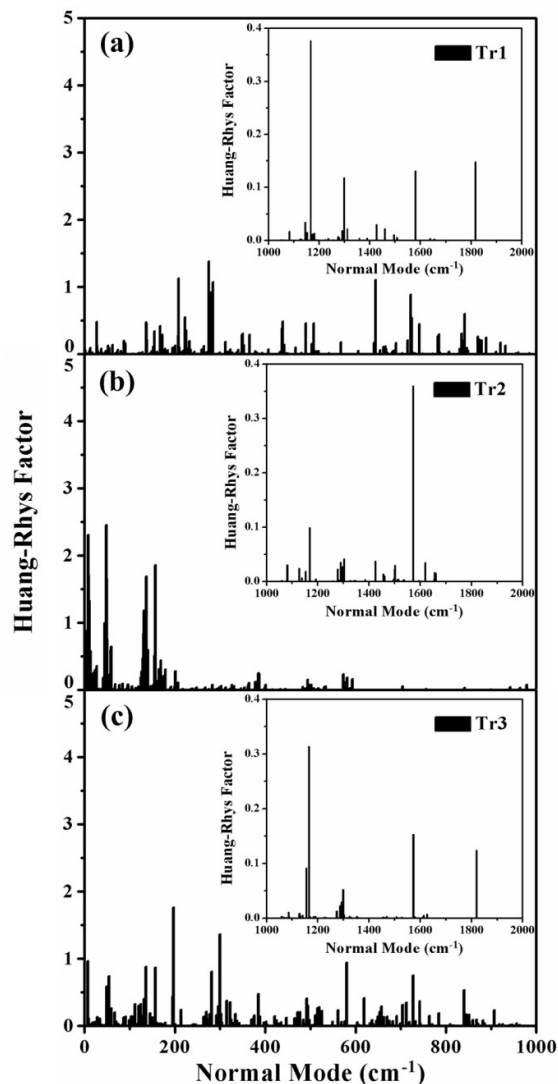
Figure 7 Calculated Huang-Rhys factors of the normal modes for Tr1, Tr2 and Tr3.

The vibrational modes of three compounds were obtained via DFT method and the Huang-Rhys factors (S) can be calculated by Franck−Condon approximation (see Table SI in Supporting Information) to obtain molecular vertical vibronic transitions. Huang-Rhys factors S characterize the vibronic coupling strength. It is clearly seen that the vibrational modes with large Huang-Rhys factors ($S>0.5$) all appear at the low-frequency regime (<1000 cm^{-1}) for all compounds. In Figure 7(b), a handful of low-frequency modes with large S mainly concentrate in a certian range (under 300 cm^{-1})

for Tr2. Nevertheless, we observed a series of vibrational modes continuously distribute in the low-frequency region (see Figure 7(a) and (c)), especially for Tr3, more low-frequency modes were expressed. A plentiful of low-frequency modes is bound to result in continuous vibronic energy level, which is adverse to the formation of four-level energy system.

Tr1

27 cm⁻¹	136 cm⁻¹	350 cm⁻¹

Tr2

6 cm⁻¹	131 cm⁻¹	157 cm⁻¹

Tr3

|			
7 cm⁻¹	270 cm⁻¹	494 cm⁻¹	727 cm⁻¹
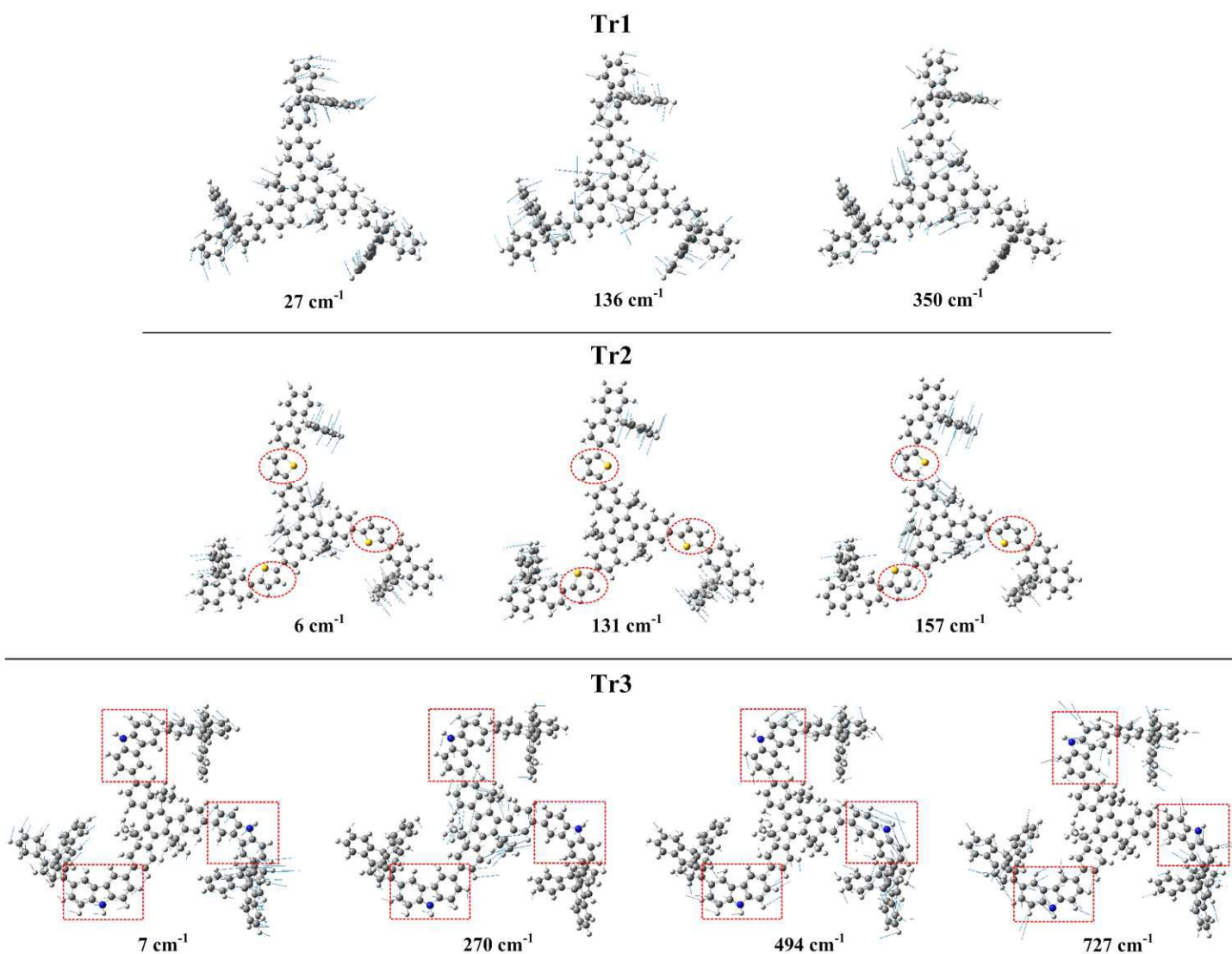
Figure 8 Calculated vibrational eigenvectors of typical low-frequency modes. The contribution of each mode to the total deformation of samples is enlarged by the same factor.

In order to clarify the relationship between the molecule structure and the normal

modes, we need to express the normal mode displacement vectors for vibrations. According to the discussion above, the major difference of vibrational modes among the three compounds derives from low-frequency modes, and Figure 8 demonstrates some typical low-frequency modes. As shown in Figure 8, because of the large dihedral angle (36.7°), the strong vibration low-frequency modes for Tr1 mainly root in the torsional and out-of-plane vibration of bulky spirobifluorene units. For Tr2, embedded thiophene moieties reduce the degree of twisting (25.6° and 26.5°), and not only the rigid thiophene does not bring out strong vibration low-frequency modes, but also it suppresses the vibration of spirobifluorene to some extent, the thiophenes seemingly "lock" the spirobifluorene, thus, the low-frequency modes with large Huang-Rhys factors in Tr2 appear under wavenumber 300 cm^{-1} with a small amount, agreement with the result in Figure 7(b). On the contrary, N-ethylcarbazole units generate a mass of strong low-frequency vibrational modes arising from the out-of-plane vibration itself due to large twist of the dihedral angles (38.2° and 39.1°), which result in a range of consecutive vibronic energy levels and unclear energy gap, as clarified in Figure 7(c). In the high-frequency vibrational modes (Figure S2 in Supporting Information), the CC stretching and CH bending in the π-conjugated moieties define the high energy vibronic peaks in PL spectra. [35, 39]

2.7. Vibronic Transitions and Four-Level Energy System
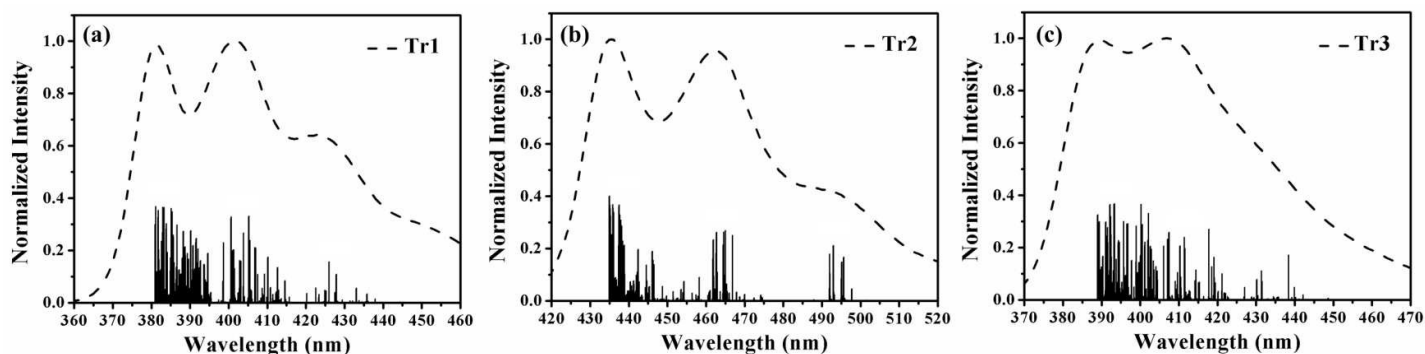
Figure 9 Calculated discrete vertical vibronic transitions (vertical columns) and experimental PL spectra (dashed lines) for Tr1, Tr2 and Tr3.

According to the analysis of transition energy (Table 2) and the relevant parameters (Table SI in Supporting Information) of vibrational modes, the vertical vibronic transition probability can be calculated (details are shown in Supporting Information), shown in Figure 9. According to the discussion in Section 2.6, with respect to Tr3, a plentiful of vertical vibronic transitions distribute between 0-0 and 0-1 vibronic peaks continuously, which is an indication of continuous vibronic energy sublevels between the zero-point vibronic level and the first vibronic level in the electronic state. For Tr1, some assignable vibronic transitions exit close to 0-0 vibronic peak as well. The vibronic transitions distribution for Tr2, presented in Figure 9(b), differs from that of Tr3. The different discrete vibronic transitions crowd together and merge into a large band attributing to minority and weak elongation of low-frequency vibrational modes, hence, a small number of discrete energy levels exist between the main peak and the vibronic subbands.
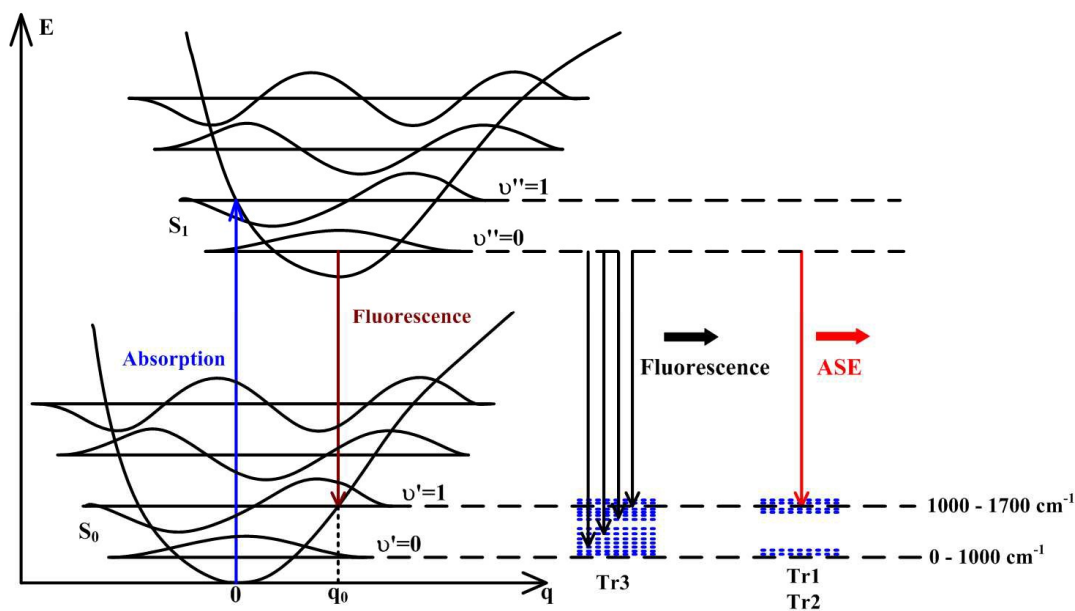
Figure 10 Four-level energy system of Tr1, Tr2 and Tr3 containing the vibronic energy levels.

The vibronic energy level system included in electronic states would be obtained on account of vibronic transitions analysis. The discrete vibronic transitions exhibit different vibronic energy level system for Tr1, Tr2 and Tr3, shown in Figure 10. When samples were photopumped, pump laser can excite the molecule from the zero-point vibronic level (υ'=0, non-equilibrium vibronic levels) to an excited vibrational level (υ''=1, Franck-Condon vibronic levels) vertically, [40] which will be followed by rapid thermal relaxation to the zero-point vibronic level (υ''=0) of the excited singlet state according to Franck-Condon principle. Hence, the energy levels of these organic semiconductors enable them to behave as a four-level energy system with population inversion between υ''=0 and υ'=1, even when most molecules are in the ground state.

Especially for Tr2, centralized discrete vibronic transitions would bring out legible energy level distribution (see Figure 10). According to four-level energy mechanism, lasing can take place via the transition from energy levels υ''=0 to υ'=1, corresponding

to the 0-1 vibronic transition. However, due to richness vibronic transitions for Tr3, the spacing of sublevels between $\upsilon'=0$ and $\upsilon'=1$ contains segments with a range of consecutive energy levels. Therefore, the dispersive vibronic transitions would terminate the formation of effective four-level energy system. In addition, the significant geometric relaxation following excitation for Tr3 (the large Stokes shift 0.64 eV, Section 2.1) directly compete with the radiative decay processes. [41] Finally, the population inversion would be difficult to achieve, and optical amplification is eliminated.

3. Conclusion

In summary, we provided the fingerprint of "four-level" system to understand the ASE mechanism based on three star-shaped compounds comprising truxene core and π-conjugated arms (Tr1, Tr2 and Tr3). Introducing the thiophene units (Tr2) between truxene core and spirobifluorene, the enhanced ASE was observed with reduced ASE threshold (down to 83 $\mu J/cm^{-1}$) compared to Tr1. However, when the thiophene was replaced by N-ethylcarbazole (Tr3), the ASE disappeared. DFT/TDDFT calculations demonstrate that the introduced thiophene improves conjugative coupling and suppresses the low-frequency vibrational modes, just like "locks" the trxuene core and spirobifluorene arms together. Meanwhile, high-frequency carbon-carbon stretching modes were enhanced in Raman spectra. Hence, the decreased low-frequency modes and enhanced high-frequency modes contribute to effective "four-level" energy system which is essential for the population inversion of ASE. Inversely, the embedded N-ethylcarbazole moieties fail to modify conjugative coupling and bring out a mass of

strongly elongated low-frequency modes, therefore, continuous vibronic energy sublevels would ruin the molecular "four-level" energy system. Our study would present a visualized picture to clarify the ASE mechanism explicitly.

4. Experimental Section and Theoretical Methodology

The thin film doped with polystyrene (PS) in a certain amount (9 wt%) of Tr1, Tr2 and Tr3 were spin-coated onto glass substrates. The absorption and PL spectra were obtained by UV-Vis spectrophotometer (HITACHI U-3010, Japan) and Fluorescence Spectrometer (fluoromax-4 spectrofluometer) respectively.

ASE measurements were carried out for thin film samples photopumped at normal incidence with a pulsed Nd:YAG laser (5.55 ns, 10 Hz) (Surelite I, Continuum Corp, USA), using the third harmonic (355 nm). The energy of the pulse was controlled by neutral density filters. The laser beam was expanded, collimated and only the central part was selected to ensure uniform intensity. A cylindrical lens and an adjustable slit were then used to focus normally onto the samples with as a stripe with the size of 7 mm×1 mm. The pump stripe was perpendicular to the surface of the samples and the emitted light was collected with Fiber Optic Spectrometer (Ocean Optics SpectraSuite, USB2000).

PLQY measurements were determined in CH_2Cl_2 using quinine sulfate ($\varPhi_{PL}$ = 56% in 1.0 M H_2SO_4 solution) as standard and PL transient decays were measured for 150 nm thickness doped films of three compounds excitation at 360 nm.

The Raman Spectra for the three samples with similar thickness (around 320 nm) were performed on a LabRam HR800 spectrometer (from Horiba Jobin Yvon) and

measured using a 600 groove/mm grating, using 514 nm emission line of a Ar+ laser.

The ground and excited-state equilibrium molecular geometries and vibrational normal modes of Tr1, Tr2 and Tr2 were calculated with DFT using the hybrid functional B3LYP and the basis set 6-31g respectively in the Gaussian 09 program package. Using the same functional and basis set, the oscillator strengths and vertical excitation energy were obtained with TDDFT in the adiabatic approximation. The vibrational frequency ($\hbar\omega_j$) and Huang-Rhys factors (S) for each normal mode are calculated using the DUSHIN program developed by Weber, Cai, and Reimers, [42] and the formula given in Supporting Information.

References:

[1] S. R. Forrest, *Nature* **2004**, *428*, 911.

[2] G. D. Scholes, G. Rumbles, *Nat. Mater.* **2006**, *5*, 683.

[3] I. D. W. Samuel, G. A. Turnbull, *Chem. Rev.* **2007**, *107*, 1272 .

[4] B. K. Yap, R. Xia, M. C. Quiles, P. N. Stavrinou, D. D. C. Bradley, *Nat. Mater.* **2008**, *7*, 376.

[5] A. L. Kanibolotsky, R. Berridge, P. J. Skabara, I. F. Perepichka, D. D. C. Bradley, M. Koeberg, *J. Am. Chem. Soc.* **2004**, *126*, 13695-13702.

[6] X. L. Meng, W. H. Zhu, H. Tian, *Prog. Chem.* **2007**, *19*, 1671.

[7] P. L. Burn, S. C. Lo, I. D. W. Samuel, *Adv. Mater.* **2007**, *19*, 1675.

[8] S. H. Wang, C. N. Moorefield, G. R. Nekkome, *Chem. Soc. Rev.* **2008**, *37*, 2543.

[9] M. D. McGehee, A. J. Heeger, *Adv. Mater.* **2000**, *12*, 1655.

[10] W. Zapka, U. Brackmann, *Appl. Phys.* **1979**, *20*, 283.

[11] H. R.Haghighi, S. Forget, S. Chenais, A. Siove, M. Castex, *Appl. Phys. Lett.* **2009**, *95*, 033305.

[12] S. Y. Ma, T. Nakajima, K.Yamashita, *Appl. Phys. Lett.* **2008**, *93*, 023306.

[13] G. Tsiminis, Y. Wang, P. E. Shaw, A. L.Kanibolotsky, I. F. Perepichka, M. D. Dawson, P. J. Skabara, G. A. Turnbull, *Appl. Phys. Lett.* **2009**, *94*, 243304.

[14] E. M.Calzado, P. G. Boj, M. A. D. García, *Int. J. Mol. Sci.* **2010**, *11*, 2546.

[15] P. A. Levermore, R. Xia, W. Lai, X. H. Wang, W. Huang, D. D. C. Bradley, *J. Phys. D: Appl. Phys.* **2007**, *40*, 1896.

[16] B. T.de Villers, B. J. Schwartz, *Appl. Phys. Lett.* **2007**, *90*, 091106.

[17] J. Mysliwiec, L. Sznitko, S. Bartkiewicz, A. Miniewicz, Z. Essaidi, F. Kajzar, B. Sahraoui, *Appl. Phys. Lett.* **2009**, *94*, 241106.

[18] R. D. Xia, W. Y. Lai, P. A. Levermore, W. Huang, D. D. C. Bradley, *Adv. Funct. Mater.* **2009**, *19*, 2844.

[19] H. R. Haghighi, S. Forget, S. Chénais, A. Siove, M. C.Castex, E. Ishow, *Appl. Phys. Lett.* **2009**, *95*, 033305.

[20] D.Schneider, T. Rabe, T. Riedl, T. Dobbertin, O. Werner, *Appl. Phys. Lett.* **2004**, *84*, 4693.

[21] S.Y. Yang, Y. H. Kan, G. C. Yang, Z. M. Su, L. Zhao, *Chem. Phys. Lett.* **2006**, *429*, 180.

[22] M. Kytka, L. Gisslen, A. Gerlach, U. Heinemeyer, J. Kováč, R. Scholz, F. Schreiber, *J. Chem. Phys.* **2009**, *130*, 214507.

[23] G. Heimel, M. Daghofer, J. Gierschner, E. J. W. List, A. C. Grimsdale, *J. Chem. Phys.* **2005**, *122*, 054501.

[24] M. M. Oliva, J. Casado, J. T. L. Navarrete, R. Berridge, P. J. Skabara, A. L. Kanibolotsky, I. F. Perepichka, *J. Phys. Chem. B* **2007**, *111*, 4026.

[25] Y. Kawamura, H. Yamamoto, K. Goushi, H. Sasabe, C. Adachi, *Appl. Phys. Lett.* **2004**, *84*, 272

[26] T. Aimono, Y. Kawamura, K. Goushi, H.Yamamoto, H. Sasabe, C. Adachi, *Appl. Phys. Lett.* **2005**, *86*, 071110.

[27] H. Nakanotani, N. Matsumoto, H. Uchiuzou, M. Nishiyama, M.Yahiro, C. Adachi, *Optic. Mater.* **2007**, *30*, 630.

[28] H. Nakanotani, S. Akiyama, D. Ohnishi, M. Moriwake, M. Yahiro, T. Yoshihara, S. Tobita, C. Adachi, *Adv. Funct. Mater.* **2007**, *17*, 2328.

[29] R. Kabe, H. Nakanotani, T. Sakanoue, M. Yahiro, C. Adachi, *Adv. Mater.* **2009**, *21*, 4043.

[30] T. Komori, H. Nakanotani, T. Yasuda, C. Adachi, *J. Mater. Chem. C* **2014**, *2*, 4918.

[31] C. Yao, Y. Yu, X. Yang, H. Zhang, Z. Huang, X. Xu, G. Zhou, L. Yue, Z. Wu, *J. Mater. Chem. C* **2015,** DOI: 10.1039/c5tc01018g.

[32] V. G. Kozlov, V. Bulovic, P. E. Burrows, S. R. Forrest, *Nature* **1997**, *389*, 362.

[33] M. D. McGehee, A. J. Heeger, *Adv. Mater.* **2000**, *12*, 1655.

[34] Y. Wang, G. Tsiminis, Y. Yang, A. Ruseckas, A. L. Kanibolotsky, I. F. Perepichka, P. J. Skabara, G. A. Turnbull, I. D. W. Samuel, *Synth. Met.* **2010**, *160*, 1397.

[35] T. Liu, C. Prabhakar, J. Yu, C. Chen, H. Huang, J. S. Yang, *Macromolecules* **2012**, *45*, 4529.

[36] N. A. Montgomery, J. C. Denis, S. Schumacher, A. Ruseckas, P. J. Skabara, A. Kanibolotsky, M. J. Paterson, I. Galbraith, G. A. Turnbull, I. D. W. Samuel, *J. Phys. Chem. A* **2011**, *115*, 2913.

[37] Q. Peng, Y. Yi, Z. Shuai, J. Shao, *J. Am. Chem. Soc.* **2007**, *129*, 9333.

[38] N. A. Kukhtaa, J. Simokaitienea, D. Volyniuka, J. Ostrauskaitea, J. V. Grazuleviciusa, G. Juskab, V. Jankauskas, *Synth. Met.* **2014**, *195*, 266.

[39] R. Scholz, L. Gisslén, C. Himcinschi, I. Vragovic, E. M. Calzado, E. Louis, E. S. Fabian, M. A. Díaz-García, *J. Phys. Chem. A* **2009**, *113*, 315.

[40] J. C. del Valle, M. Kasha, J. Catalán, *J. Phys. Chem. A* **1997**, *101*, 3260.

[41] C. R. Belton, A. L. Kanibolotsky, J. Kirkpatrick, C. Orofino, S. E. T. Elmasly, P. N.

Stavrinou, P. J. Skabara, D. D. C. Bradley, *Adv. Funct. Mater.* **2013**, *23*, 2792.

[42] Z. L. Cai, J. R. Reimers, *J. Phys. Chem. A* **2000**, *104*, 8389.